Circumferential Guided Wave EMAT System for Pipeline Screening using Shear Horizontal ultrasound

Matthew Clough [1, 2 a)], Matthew Fleming[2] and Steve Dixon[1]

[1] *Physics Department, University of Warwick, Gibbet Hill Road, Coventry CV4 7AL, UK*
2 Sonomatic Ltd, Dornoch House, The Links, Birchwood, Warrington, Cheshire, WA3 7PB, UK

[a)] Corresponding author: M.Clough@warwick.ac.uk

Abstract

The use of guided waves is now widespread in industrial NDT for locating metal loss in pipelines, that manifests as pitting, corrosion and general wall thinning. In this paper, a screening technique is assessed in terms of defect detection and defect sizing capability. Shear Horizontal (SH) guided waves propagate circumferentially around the pipe whilst the scanner is moved axially along the length. This type of tool is preferable to other methods, being applied to the exterior of the pipe, without requiring full circumferential access, and is able to operate through thin coatings (up to 1 mm thick). It is designed to provide a pipe screening tool for petrochemical pipelines both topside and subsea, particularly for detecting defects at pipe support areas. The system's efficacy in terms of detection and sizing of defects is considered via experimental measurements on artificially induced defects and in service corrosion patches, with results compared to finite element modelling of the interaction of the guided waves with artificial defects. Finite element modelling has

been used to better understand the behaviour of different wave modes when they interact with defects, focusing on the mode conversions and reflections that occur.

Keywords: EMAT; Guided waves; Shear Horizontal; Pipelines; Screening

1. Introduction

Ongoing condition monitoring and NDT of carbon steel pipelines that carry product in the petrochemical industries is essential in order to prevent catastrophic failure of these pipelines. Monitoring of the condition of these pipes focusses on detecting and quantifying wall thinning that is caused by internal or external corrosion of the sample. External corrosion in these samples is generally found at positions where water is trapped and can pool, leading to damage to coatings, pitting and wall thinning type corrosion [1,2]. This corrosion often occurs at pipe support areas, where there is not full circumferential access to the pipeline, or at the contact with another surface such as the base of a pipeline that is seated on the sea bed. The nature of these pipelines means that there are often large lengths of pipe which need to be tested in one measurement, and so a screening method that is rapid and reliable is required, to provide an assessment of the level of corrosion in the pipeline. In industry, the preferred methods for these types of inspections are long range guided wave inspections [3] or the use of inline pipeline inspection gauges (pigs) [4] that travel through the interior of the pipe taking measurements of wall thickness. These are often confirmed with subsequent ultrasonic thickness gauging of corroded areas [5]. However, these techniques have limitations, in that the long range guided waves are generated via a collar of piezoelectric transducers in pulse echo operation [3,6], which requires full

circumferential access. Smart inspection pigs may require processing shut down [7] and that the pipe is capable of having a pig installed, which is not possible in all cases.

This paper describes a much shorter range tool for the screening of pipeline in general, and for detection of corrosion under pipe support areas or others with a lack of direct access to the defect area. It describes the operation of Shear Horizontal (SH) guided wave, Electromagnetic Acoustic Transducer (EMAT) systems for general pipe screening, with defect detection, sizing and positioning capabilities. The limitations in terms of the defect detection and sizing are considered to optimize inspections. Finite element models are presented to aid interpretation of experimental results and to illustrate similarities and differences between realistic defect shapes and the shape of calibration defects, in order to investigate whether the calibration defects used are actually valid representations of realistic defects.

2. System design and characterisation

The pipe screening system presented here consists of a scanning rig to which two SH guided wave EMAT probes are fixed at a known separation as shown in Figure 1. The probes are then operated in a pitch catch configuration, with ultrasonic guided waves generated that propagate in the circumferential direction around the pipe in both directions. The scanning system is centred at the top of the pipe to provide a known travel distance to the base of the pipe and between the two probes. Their positioning is designed to separate the signals received into a short path (SP) signal that corresponds to travel over the top of the pipe, and a long path (LP) signal that travels around the base of the pipe as illustrated in Figure 2a. The scanning rig is then moved axially along the pipe's length to provide an

encoded scan that has interrogated the sample at all points around the circumference and length. The use of guided waves means that the ultrasound can be generated a distance away from the defect area and the dispersive properties of these waves can be used to investigate the condition of the sample.

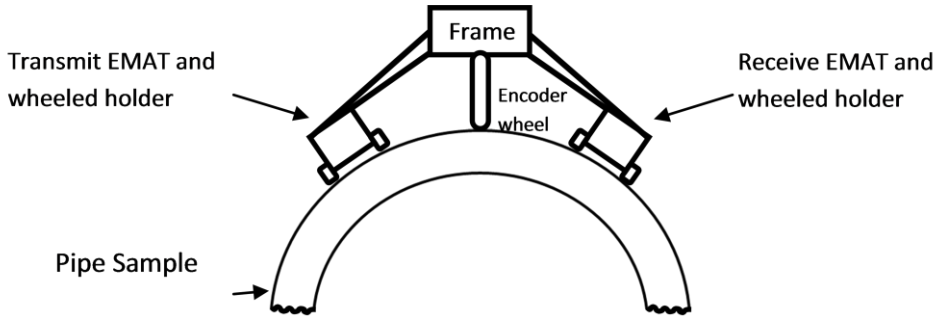

Figure 1 Schematic diagram of the scanning rig used to hold the transducers for pitch catch style screening scan of a sample (not to scale).

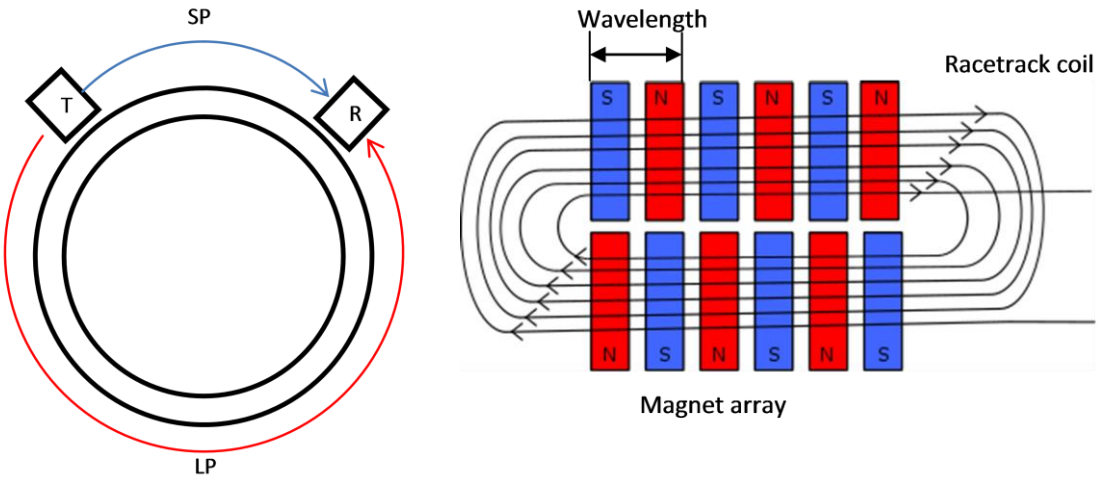

a) b)

Figure 2 a) Schematic diagram of the transmit (T) and receive (R) EMAT probes on a pipe surface illustrating their positioning on the pipe surface and the corresponding short path (SP) and long path (LP). b) Schematic of the periodic permanent magnet (PPM) array EMAT probe showing the array of permanent magnets at fixed separation to define a nominal wavelength of the probe and a racetrack shaped excitation coil beneath the array which is pulsed with an excitation signal to generate the desired wave mode.

The probes used in this paper are EMATs of the periodic permanent magnet (PPM) array type [8], used to excite SH waves of a particular nominal wavelength in the sample defined by the magnet spacing. These probes consist of an array of permanent magnets of alternating polarity that are separated from each other with a constant spacing between magnets, the form of which is illustrated in Figure 2b. The spatially periodic magnetic field they produce then interacts with the eddy current induced in the sample by a racetrack coil below the magnet array. The Lorentz and magnetostrictive forces generated by this arrangement generate a shearing force at the surface of the sample, with the Lorentz force being the dominant mechanism in the generation of ultrasound within the sample [9,10]. The spacing of the magnets in the array sets the nominal wavelength at which the probe can generate ultrasound, and hence where various modes can be excited by changing the frequency of the excitation signal. The interaction of the generated wave modes with defects present in the sample can then be used to find defects.

SH guided waves are a family of dispersive wave modes whose characteristics depend on the frequency, sample thickness and bulk shear wave speed of the sample. For low frequencies, only the SH0 mode exists, but for higher frequencies, a range of modes can exist depending on the frequency and wavelength combination used in the experiment. It is important to examine the dispersive behaviour of these waves when choosing a position on the dispersion curves to operate. One must consider which of the waves are required and the dispersion (or lack thereof) that is desired in the generated signals. Operation with a larger frequency bandwidth can complicate the signal, due to introducing further modes into the sample [11], but it can also produce more information about the presence of defects when using different modes. The modes that an EMAT will generate with a given

frequency of excitation signal can be visualized on phase velocity dispersion curves for the sample in question, with the phase velocity being a function of the frequency thickness product in the sample, so that different thickness samples have different velocities for a given frequency. The points where guided waves can be most efficiently generated in a sample for a given wavelength probe can be shown on phase velocity dispersion curves where a line of constant wavelength intersects the different mode curves. The phase velocity dispersion curves for SH guided waves in a plate include multiple symmetric and anti-symmetric modes, the order of which is defined by *n* which for a frequency, f, plate thickness of $d=2h$ and a bulk shear wave speed c_s, the phase speed c_p is given by:

$$c_p(fd) = \pm 2c_s \left\{ \frac{fd}{\sqrt{4(fd)^2 - n^2 c_s^{\,2}}} \right\} \tag{1.1}$$

With the corresponding group velocities given by:

$$c_g(fd) = c_s \sqrt{1 - \frac{(n/2)^2}{(fd/c_s)^2}} \tag{1.2}$$

These equations produce dispersion curves such as those shown in Figure 3a, with the symmetric and antisymmetric modes and a dashed line corresponding to a line of constant wavelength is superposed on the dispersion curves. This constant wavelength dashed line corresponds to the nominal wavelength of the EMAT, as defined by the magnet spacing.

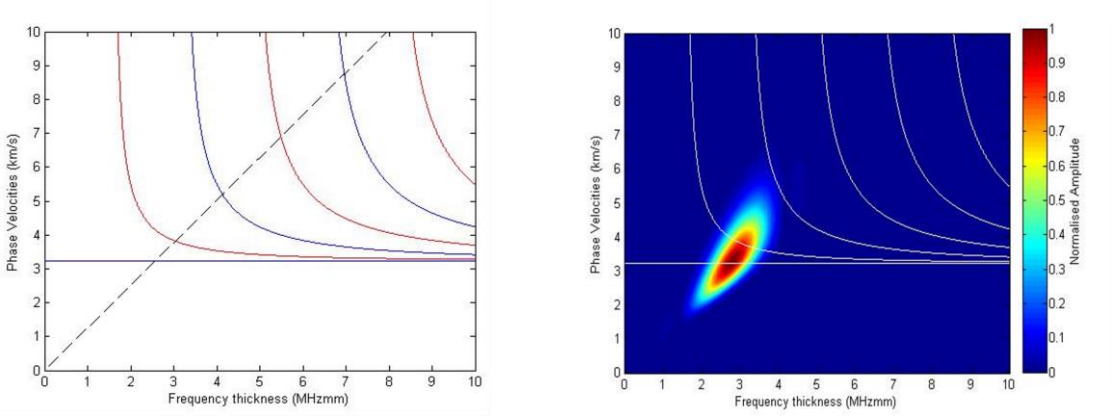

a) b)

Figure 3 a) Phase velocity dispersion curves for a 7 mm thick steel plate and the excitation line for an 8.8 mm nominal wavelength probe. b) Area of operation for the probe excited with a 5cycle tone burst on a 7 mm thick sample. Different guided waves modes will be generated when this operation area coincides with a wave mode curve.

In practical application of the probe however, the operating range is not limited to the points at which the line of constant wavelength intersects with the SH modes on the phase velocity dispersion curves. Instead a range of operation wavelengths and frequencies exist due to the spatial and frequency bandwidths inherent from the magnet spacing in the probe and the current pulse used to drive the system. The convolution of the two different bandwidths determines an area of operation for the probe, and careful consideration of the EMAT's spatial bandwidth and frequency bandwidth of the signal are necessary [11].

In this case the convolution of the spatial bandwidth of the wavelengths from the selected 8.8 mm probe and the frequency bandwidth generated by the 5 cycle tone burst used to excite the transducer coil, gives an area of operation on the dispersion curves as shown by Figure 3b, where the colour scale represents the relative strength of the generated signal at each point, with respect to the peak frequency and wavelength combination. This

illustrates how the actual operation of the probe is spread over an extended area on the dispersion curves, such that more than one mode, each with a range of frequencies can be excited for a given wavelength probe and current drive pulse. It also explains how this approach can generate multiple modes in a sample when using a wider band signal. This gives a more complete view of the range of values at which these probes operate and can be subsequently used to explain the excitation of ultrasound in more detail. This becomes much more relevant when pipe samples are of interest, as the curvature of the sample changes the dispersion curves away from the well defined case presented for a plate [12]. The 5 cycle excitation signal as described is a limitation imposed by the hardware used to generate the signal. This equipment needs to be portable and battery powered in order to be a feasible system for the chosen use, so the pulser sets a practical limit on the number of cycles that can be used in the tone burst. The effect of this is that the signal is relatively broadband and spans a range of values on the dispersion curves, which can make the resulting signals more dispersive and difficult to interpret, but difficulties would also arise when using a greater number of cycles due to the elongation of these signals making the isolation of different signals more difficult. The 5 cycle tone burst used here is therefore a compromise between the energy requirements of the system and the desired bandwidth range of the generated signal.

In a plate sample, the dispersive behaviour is determined by the frequency, thickness and bulk shear wave speed in the sample. This dispersive behaviour is sometimes assumed to be the same in a pipe, by using the concept that a plate can be considered an unwrapped pipe. For accurate thickness measurements on the pipe, the correct dispersion curves should be used, as the dispersion behaviour is dependent both on the thickness of the sample and the

outer pipe wall radius due to the curvature of the pipe [13]. The propagation of guided waves in the circumferential direction of a sample is more complex than in the plate, generating solutions that contain Bessel functions. The generation of these equations will not be presented here in detail and can be found in the literature [12–14], but in general the characteristic equation for circumferential SH waves in a single layer annulus is given by

$$\det\left(D\left(p,\omega\right)\right)=0 \tag{1.3}$$

where the eigenvalues of this, form the dispersion curves in the pipe in the form of frequency-wavenumber curves. Here p is the angular wavenumber and ω is the angular frequency and D is the coefficient matrix:

$$D\left(p,\omega\right)=\begin{bmatrix} J_{p-1}\left(k_s r_1\right)-J_{p+1}\left(k_s r_1\right) & Y_{p-1}\left(k_s r_1\right)-Y_{p+1}\left(k_s r_1\right) \\ J_{p-1}\left(k_s r_2\right)-J_{p+1}\left(k_s r_2\right) & Y_{p-1}\left(k_s r_2\right)-Y_{p+1}\left(k_s r_2\right) \end{bmatrix} \tag{1.4}$$

Where J is a Bessel function of the first kind and Y is a Bessel function of the second kind, with r_1 the inner radius and r_2 the outer radius and k_s the circular wavenumber of a bulk shear wave. The frequency wavenumber curves can then be manipulated to obtain the phase velocity curves and subsequently the group velocity dispersion curves.

For the samples considered here of a 7 mm wall thickness and a 540 mm outer circumference carbon steel pipe, the dispersion curves start to diverge from the flat 7 mm thick plate dispersion curves as shown in the group velocity dispersion curves of Figure 4. Whilst the cut off frequency thickness for each mode remains the same for the flat plate and curved pipe as defined in equation 1.5, there are some significant differences in the dispersion characteristics, as can be seen in Figure 4.

$$\left(fd\right)_n = nc_s/2 \tag{1.5}$$

The SH0 mode propagating around the pipe circumference is no longer non-dispersive at all frequencies and so will show some dispersive behaviour. The higher order mode dispersion curves also differ from the flat plate properties, especially in the 'knee' area of the dispersion curves where these probes are operating, due to the nominal wavelength of 8.8 mm that the probes have been designed to operate at. The differences between the phase and group velocities for the 7 mm thick plate and the corresponding 7 mm thick, 540 mm circumference pipe sample are shown in Figure 4. The differences in these curves emphasises the need to use the correct pipe dispersion curves, as the same excitation signal for the probes will generate a different velocity wave in the different geometry samples. This will affect the time of arrival of the generated guided waves at the receiver, such that an attempt to use the plate dispersion curve to assess time of arrival of waves generated in the pipe will not be accurate. This in turn adds more uncertainty to any assessment of defect areas as this relies on a change of arrival time relative to the defect free arrival time.

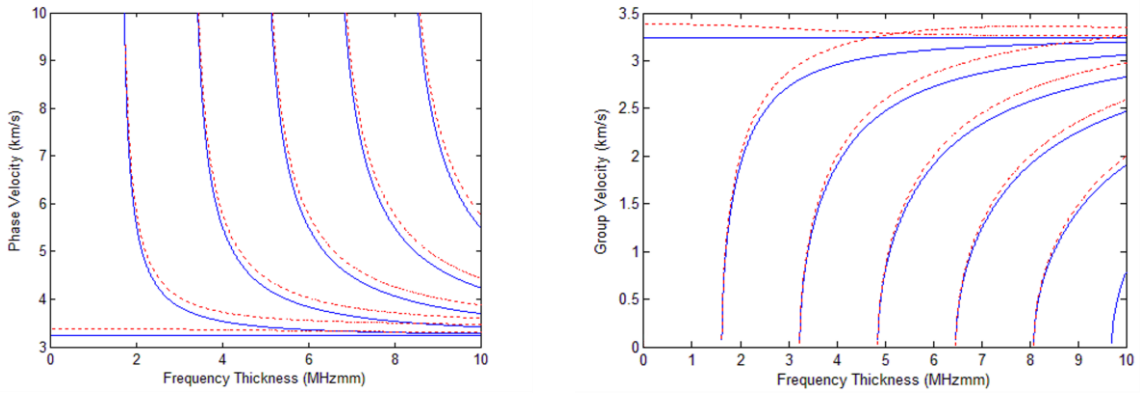

a) b)

Figure 4 Comparison between a) the phase and b) group velocity dispersion curves for a 7 mm thick plate (solid blue) and a 7 mm thick 540 mm circumference pipe sample (dashed red).

In the current presentation of this work, the presence and severity of a defect is defined with reference to the cut off thickness of the SH1 mode in the material. Using the fact that there is a lower bound of frequency thickness product below which the SH1 mode cannot propagate without disruption through the defect area, we can set limits as to what will be seen in a scan.

The scans here are put into one of three categories. If the signal is unaffected, showing the same arrival times and amplitudes as the area with no defect then the area that is scanned can be said to be defect free. If the behaviour of the SH0 or the SH1 mode changes, it can be said that a defect is present in the sample. If the defect causes a slowing of the SH1 mode so that the mode arrives later than the area with no defect then there is a defect present, but the depth of the defect is not enough to take the sample thickness below the SH1 mode cut off. If there is a change in the behaviour of the SH1 mode such that the mode is removed from where it was expected in the sample or if the signal arrives faster than the expected SH1 arrival time then there is a defect present that has a depth that is below the SH1 mode cut off and so is a more extreme defect resulting in the mode conversion of the SH1 mode to an SH0 mode or reflection of the SH1 mode at the edges of the defect. In these circumstances it is important to consider what happens to the energy of the SH1 mode as it reaches the defect and will be considered in the simulated data that is presented later to determine the extent of reflection and mode conversion of the modes.

3. Experimental sample

Experimental trials and validation of the system have been carried out on a number of samples both with artificial defects and in service corrosion style defects, with a range of

coating types and thicknesses. The sample that will be considered predominantly here is a 7 mm thick carbon steel sample, with a circumference of 540 mm and a defect area that has been artificially induced as an area of wall thinning through removal of the wall material. This defect has an axial extent of 48.56 mm and a 44 mm circumferential extent, with a remaining wall thickness of 2.2 mm. The transducer trolley is centred at the top of the pipe with the defect at the base of the pipe as would be the case in a pipe support inspection. The geometry of the defect's edges and the depth throughout the defect is known to affect the levels of mode conversion and reflection of the various modes. In order to supplement the experimental data and clarify the extent to which these phenomena occur, a range of different defect geometries is used in a finite element simulation to give an approximation to the experimental situation.

4. Simulation Setup

A finite element model of the system was generated to isolate aspects of the wave behaviour and obtain a better understanding of the system performance. The input to the finite element model for ultrasound propagation in a sample was generated by formulating a model of the transducer in COMSOL, as has been described previously [11], to ascertain the form of the pressures that such a transducer exerts on the surface of a sample. This surface pressure profile is important as it sets the spatial bandwidth of the system, with a wider spatial bandwidth, meaning that undesired modes from the dispersion curves are excited. The displacement profiles from the COMSOL modelling are used to provide directional pressure loads for a 2D surface in a finite element model in the commercial software PZFlex. PZFlex is an explicit time domain solver that is well suited to the

modelling of ultrasonic wave propagation, with rapid simulation times. It determines the time domain response of a system to loading, to provide time domain results that are close to that which would be obtained in an experiment. The application of the calculated pressures within PZFlex on the surface of a pipe structure leads to the generation of an ultrasonic signal in the model that is analogous to the experimental signal. The use of the excitation signal modulated by the amplitude of the spatial profile at each point and an analogue of the same at the receiver position allows transmission and reception in the model that is a good approximation to the behaviour seen in the experimental EMAT results.

The 2D model can be used to visualise the propagation of the SH waves at all points on the circumference of a pipe sample. Since the model is presented in 2D, this represents the signal at a single point along the length of the pipe, providing both pictorial and quantitative information about the propagation of these modes in the circumferential direction. This method of viewing the waves at one position on the axial length of the pipe was chosen to investigate the reflection and mode conversion behaviour of these guided waves in a sample, and so ignores other factors such as diffraction and scattering in the axial direction. This will mean that the results will not necessarily be very close to the experimental results, but could be used to compare how much of an effect other parameters from the 3D situation have on the scans.

The choice of this 2D geometry is intended to clarify what happens to an incident wave when it comes into contact with a defect area of the pipeline. This is important, as experimental scans of samples containing defects show a change of arrival time and amplitude of the different wave mode energy when the experimental rig is moved over the

defect area. The simulation is intended to calculate where this energy is redistributed to, if the options of diffraction and scattering axially into the bulk of the material are neglected. This has been considered previously for the flat plate case [15,16] and the axial direction of a pipeline [17], but is less well defined for the circumferential case.

5. Results

Encoded scans were taken on the pipe sample by moving the experimental scanning rig along the axial length of the pipe and exciting the probe with the 5 cycle tone burst mentioned previously. This generates both the SH0 and SH1 modes at different velocities and frequencies that propagate around the pipe circumference. Given that the separation between the transducers and the pipe circumference are known, a short path and a long path signal can be identified. The use of a pipe with a single wall thinning defect surrounded by a clear area where there is no corrosion, enables one to quickly identify areas of corrosion. This can be highlighted by the change in the amplitude of a mode, the change in arrival time, or the absence of a mode from where it would be expected on the scan. When the defect area has a thickness that is below the cut off thickness, the SH1 mode will not be able to propagate as a pure SH1 mode under the defect and can mode convert to SH0 and will propagate through, or will be reflected or mode converted at the edge of the defect and not travel through the defect area. In the experimental measurement, the energy could also propagate away from the receive transducer due to effects such as diffraction and scattering of the beam axially away from the reception point.

Scans of the pipe's length are presented in both the raw data form (Figure 5a) and a processed data form (Figure 5b). The processed data form is achieved by gating the A scan

data into several sections, each containing one or more of the modes and then normalising the data in these sections to the highest magnitude value received. The purpose of this is to emphasise the extra structure that arises when a defect area is reached by making it more visible in the colour scaled image.

From a qualitative view of the data it would appear that the expected SH1 mode long path signal is not detectable in the defect area, with the energy being redistributed into an ultrasonic signal that arrives earlier than the SH1 mode long path and much later than the expected signal. This is consistent with a combination of a mode converted signal that has travelled through the defect area and a reflected wave from the edge of the defect respectively, and modelling of this situation has confirmed the validity of this assumption.

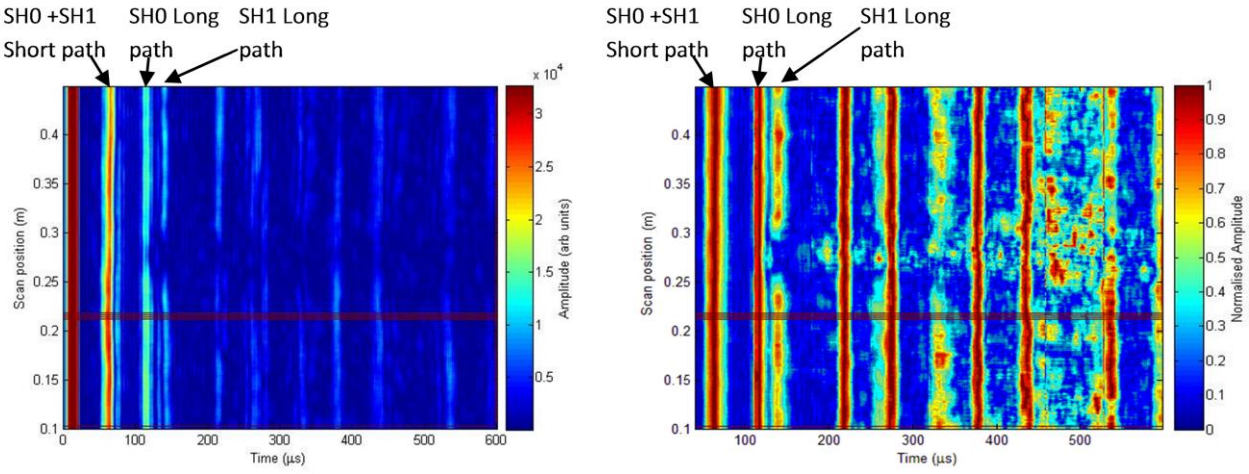

a) b)

Figure 5 Encoded circumferential scans of the sample as the transducers are moved axially along the pipe with different levels of processing, a) raw data image of the pipe scan with defect area highlighted and b) After processing to highlight defect areas and different coherent signals received in defect areas, intended to aid visualisation of the data.

Regardless of what happens to the redistributed signal energy at the defect, the presence of the defect can be seen in either version of the scan from the comparative change in the scan appearance compared to the clear section appearance. This change in amplitude of the mode in the defect area can be used to quantify the axial length of the defect. In order to determine the axial size of the defect, the Root Mean Square (RMS) of the SH1 mode at each point along the pipe scan can be calculated by taking the square root of the average of the squares of the waveform values [18]. This value can then be normalised to the average value of the mode in a clear area, so that an SH1 mode amplitude profile along the pipe can be found. This profile will show the presence of a defect by a dip in amplitude at the defect position. This analysis is effective at finding the presence of defects and the axial extent can then be determined by finding the minima of the defect profile and searching to either side of the minima to find the first position where the profile regains an amplitude similar to that of a clear area. An estimate of the defect's axial length can then be obtained by subtracting the active area of the probe in the axial direction from the length of the disruption to the amplitude profile. For an exact measurement of this axial length, the beam width at the defect position would be used, but modelling of the beam profile (not presented here) showed that the axial size of the probe was a good approximation to this on the pipe circumferences tested. Axial sizing is possible even in defects that are comparable to the axial size of the transducer and below.

This defect profile is illustrated in Figure 6, where the profile from a defect whose axial length is comparable to the transducer size is shown in a) and the profile from a defect of much larger axial size than the transducer shown in b). Scans to show defects with smaller axial lengths than the transducer active area are possible by analysing how the modes

change from what would be expected from a clear area. In such cases it is more likely that waves will diffract around the defect and so the sizing of such defects is less reliable.

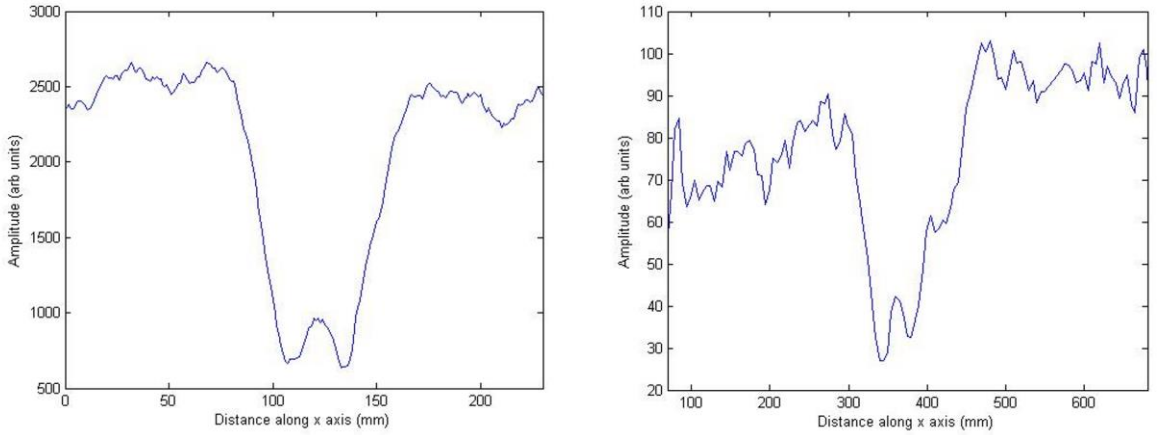

a) b)

Figure 6 Relative amplitude of the SH1 mode as the scanner is moved axially along the pipe showing the decrease in amplitude of the mode as the defect is reached. The profile in a) is for a defect of 48 mm length with a 40 mm active area transducer and b) is for a defect of 145 mm axial extent with the same transducer active area.

In trials, this method has been proven to effectively locate defects, with a good performance on corrosion patch style defects. In the trials all desired defects were located reliably with no false calls. Axial sizing was effective down to 20 mm diameter defects, with smaller defects than this difficult to separate from the background especially if the defect depth is small. Once a defect is detected, its severity can then be classed into one of 3 categories as mentioned previously, depending on the extent of redistribution of the SH1 energy when incident on the corroded area.

This screening technique can also give an indication of where a defect is situated on the circumference of the pipe. If the defect is between the transducers at the top of the pipe, then the effect it has on the ultrasonic signals will be seen in the short path signals and if

the defect is between the transducers on the rest of the circumference, its effect will be seen on the long path signal. This provides a means of sectioning the pipe circumference to give a rough positioning of the defect. With the samples tested and the transducer used, the different modes are usually separated in time in the long path signal and so the defect is easily visible. Defects in the short path are less easy to identify, with the waveforms mixing due to their similar arrival times. Identification of short path defects becomes simpler if a larger diameter sample is inspected, as the two modes then have a greater time separation in the scans.

Difficulties also arise when there is a defect directly beneath the transducers, as corrosion products from the defect can alter the lift off of the probe from the surface. This will not be common in the general operation of the tool but if it occurs it can be extreme enough to entirely remove the signal from the received scan. The effect of the change of lift off reducing the ultrasonic signal generated at these points could obscure other defects and so limits this technique for a pipe surface of variable surface geometry. However, if the inspection time is not limited, this can be overcome by adjusting the position of the probes on the surface to avoid the defect and rescanning. A further weakness the technique suffers is the lack of ability to differentiate between one or multiple defects at the same point axially but different positions circumferentially if they are within the same path between the transducers.

An example of the potential for circumferential positioning of defects using the system is shown in Figure 7. This sample is a much larger diameter pipe with a circumference of approximately 863 mm, a nominal wall thickness of 6.4 mm with a 1 mm thick polymer coating applied to the external surface of the pipe. This sample has a range of in service

defects present that occur at varying positions around the circumference of the pipe. These are corrosion patch style defects with the corrosion scabs still in situ. The scan was carried out as previously defined, although in this case a scanning rig was not available and so the scan was carried out manually with 5mm steps of the transducer. The presence of defects can be highlighted by their effect on the expected signals as in the previous example, but here it is apparent that some defects affect the short path signal and some affect the long path signal. Specifically defects 1,2,3,9 and 12 affect the long path signal whereas 4,5,6,7,8,10 and 11 affect the short path of the signal. Defects 4, 8 and 11 can be seen to be different to all the other defects because they are areas where the surface geometry has changed due to a defect being directly beneath the probe, which has altered the lift off of a probe, resulting in a less optimal generation of ultrasound within the sample.

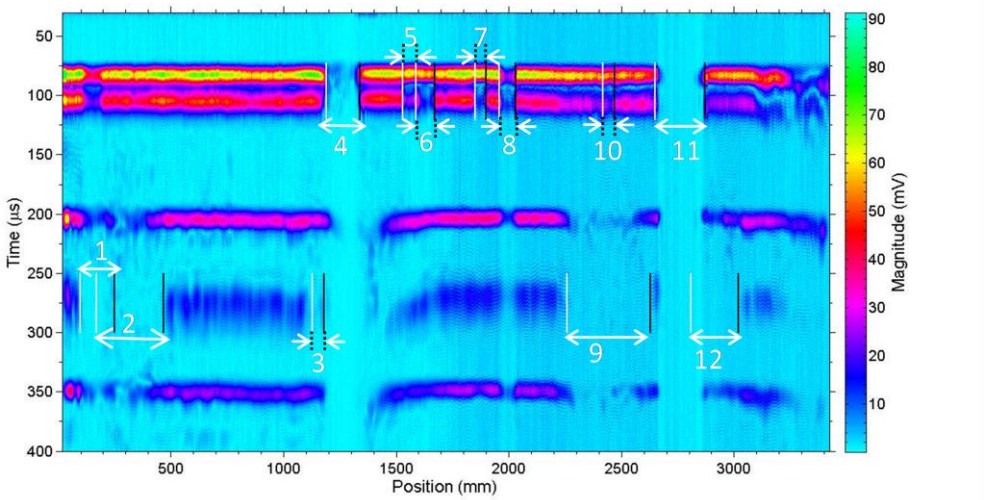

Figure 7 Encoded scan of coated pipeline with in service corrosion defects present, whether these defects affect the short or long path signals signifies if they are situated around the top sector of the pipe between the transducers or on the base of the pipe between the transducers.

6. Finite Element Modelling

Finite element modelling of a two dimensional slice of the 540mm circumference pipe was carried out to examine the behaviour of ultrasonic SH guided wave signals travelling around the circumference of a pipe sample. The simulation was designed so that both the transmission and reception of the ultrasonic signals would mimic that seen in the experimental measurements. The simulation is intended to confirm the conclusions about the removal of the SH1 mode energy and its redistribution elsewhere within the received signals. The results from the simulation assume that the sample has no axial extent, so that all of the energy that is input can be received at the transducer, with none of the effects of diffraction or scattering axially into the bulk considered.

The simulation was established so that both the A scan data from an inspection, and a visualisation of the modes as they propagate around the pipe circumference were available. Hence different waveforms in the ultrasonic signal could be identified by their arrival time, frequency and the displacement profile of the mode through the thickness of the sample as the SH0 mode and the SH1 mode have characteristic displacement profiles through the thickness of a sample that can be used to differentiate them from one another. A scan of the pipe structure with no defect present was taken from the simulation and compared to the experimental data and the theoretical dispersion curves. Both the frequency content of the signals received in the simulation and the arrival times of the different modes were found to correlate well with both experimental measurement and analytical dispersion curve values.

Simulation of the presence of defects in a sample that change the sample thickness, and as a result change the received guided wave signals, was undertaken using a range of different defect geometries to calculate their effect on the received signals. The three main

cases investigated are shown in Figure 8 and represent different situations that can be seen in calibration defects used in industry and more realistic defect shapes. The first two defect types shown in Figure 8 a) and b) are intended to represent the types of calibration defects that are often used in industry to represent defects, and are not intended here to represent real corrosion patches. The defect in a) has an abrupt change from the full thickness of the pipe to the full depth of the defect, which then remains constant, following the curve of the pipe until it reaches the end of the defect where there is another abrupt change from the full depth of the defect back to the full thickness of the pipe. This is analogous to having a flat plate with a flat bottomed hole in it and bending it into a pipe shape. The defect in b) is intended to represent a flat bottomed hole induced directly into the pipe sample such that the beginning and end of the defect is an abrupt edge but the depth doesn't become the full depth of the defect until the centre of the defect is reached. Simulations carried out with these style of defects with abrupt edges caused much stronger reflection of the SH0 mode than was seen experimentally both at the initial edge of the defect and once the wave reached the far edge of the defect, causing an effective reverberation within the defect and introducing a range of other reflection type waveforms that are not seen in the experimental data of real corrosion patches.

This illustrated the difference between artificially induced corrosion patches and real corrosion patches and emphasises the need for caution when designing simulated corrosion patches to test such systems, that may be far removed from the true shape of a corrosion defect. The defect geometry shown in Figure 8c was designed to provide a more relevant corrosion patch geometry to that of a real corrosion patch, with a sloping beginning and end down to the maximum depth of the defect. The lack of abrupt edges in this case allows for

the waves to propagate with less reflection and more energy remaining in the modes that propagate through the defect length either as pure SH0 and SH1 modes or as mode converted signals. The data output from the simulation of this more realistic defect will be used to compare with the experimental measurement to both validate the defect model and confirm where the extra experimental signals come from.

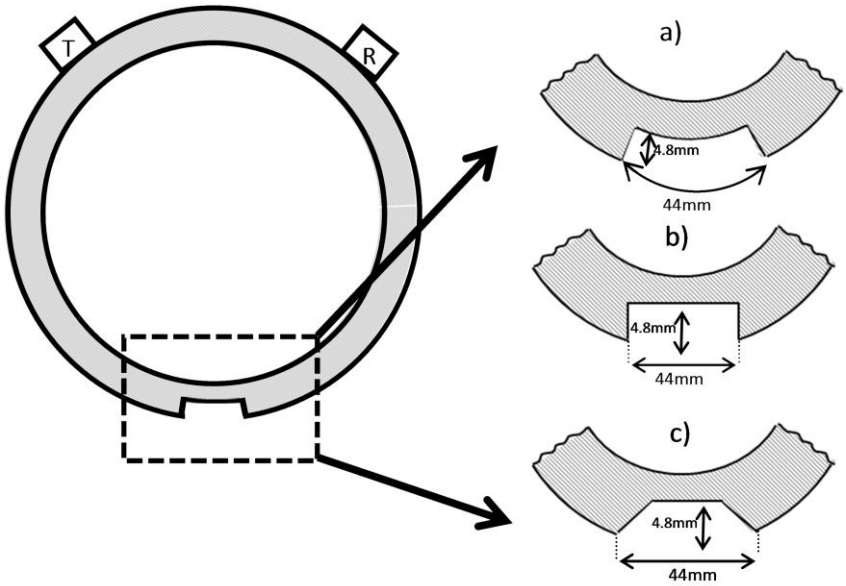

Figure 8 Schematic of the sample used in the simulations and the geometry of the different defects investigated. The sample and defects had the same dimensions as the representative artificial defect sample.

For reference, the experimental A scan for the defect area in the sample on which the simulation is based is provided in Figure 9a. This shows an initial dead time for the transducer followed by the almost simultaneous arrival of both the SH0 and SH1 modes from the short path of travel over the top of the pipe due to their similar speeds at the area labelled 1). This is followed by a long path SH0 signal at 2) and what appears to be a small amplitude signal corresponding to a mode converted SH1 mode at 3). A reflected signal from the edge of the defect then appears at 4) just before the signal corresponding to the SH0 mode that has travelled the entire circumference of the pipe plus a short path between

the transducers at 5). The assumptions about the origin of these signals were then confirmed using both the simulated A scan data obtained as in Figure 9b and the visualisation of the propagating modes provided in PZFlex.

The simulated data shows a similar pattern of wave arrivals to that of the experimental measurements, with a few inherent differences that should be noted. Firstly there is no initial dead time as a real transducer isn't used, and secondly there is no experimental noise in the simulations so the waveforms will be clearer. This is emphasised by the fact that the effects of material attenuation have been ignored in the simulated data, so that the waveforms are shown as full amplitude with no decay with distance. Thirdly, the simulation assumes no axial extent of the sample so that all the energy in the signal that is redistributed as a result of the waves interacting with the defect is captured. This is because effects such as diffraction and scattering into the bulk in the axial direction are not permitted in the model used.

Despite these differences, the simulated and experimental data show good agreement, with the same wave arrivals occurring at the appropriate arrival times. The waveforms seen in the simulated data show the short path SH0 and SH1 modes occurring together as before at 6), followed by the long path SH0 signal at 7). The next waveform was then confirmed to be a mode converted signal that travels as an SH1 mode to the defect, mode converts to an SH0 mode under the defect and then converts back to the SH1 mode at the far side of the defect at 8). This is because the remaining thickness of the sample in the defect area is below the cut off thickness of the SH1 mode. Thus the SH1 mode cannot propagate freely through the defect area, but must instead redistribute its energy to become an SH0 mode under the defect and then convert back into SH1 when the thickness of the sample becomes

above the cut off thickness again. There follows two other wave arrivals that represent the reflected portions of the SH0 and SH1 modes as they are incident on the defect edge at 9) and 10). These appear at a much higher relative amplitude than is seen in the experiment, due to the two dimensional nature of the simulation retaining all the energy in the signal with no opportunity for it to be distributed into the axial bulk of the sample. The simulation then shows the same SH0 signal for travelling a whole circumference plus the short path distance as seen in the experimental measurements at 11).

The outcome of the simulation has shown a good correlation with the experimental measurements, and is an effective way to identify the origin of the different signals in a scan that arise when a defect is present. It has also clarified the differences between realistic corrosion patch style defects and the more artificial geometries that are often used for the calibration of systems. It highlighted some of the differences that may arise between artificial and real corrosion patch shapes and the caution needed when comparing the two.

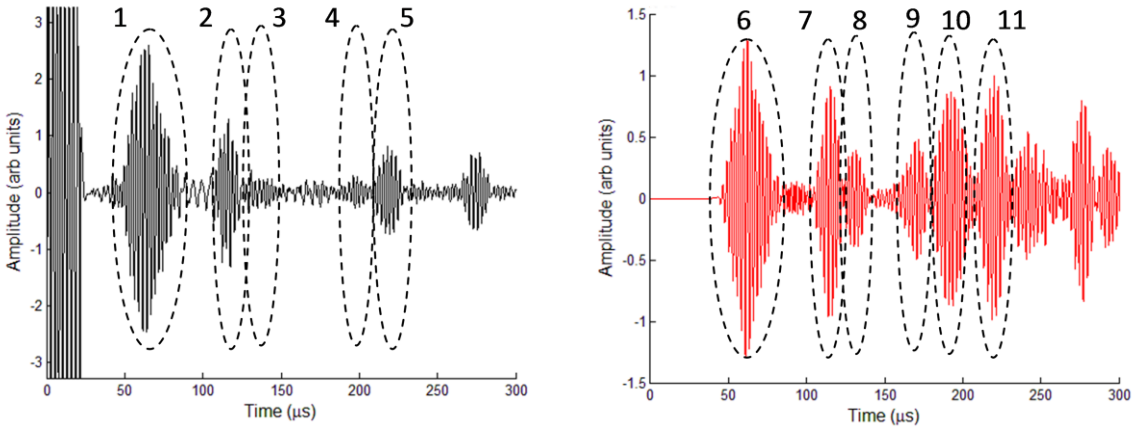

a) b)

Figure 9a) Experimental A scan from the defect area and b) simulated A scan from the defect with different modes highlighted.

This model can now be used to simulate other circumstances of interest such as a variation in defect circumferential extent or different defect depths and the positioning of the defect around the circumference of the pipe.

7. Conclusions

The system provides an effective screening tool for defects in pipe samples of different diameter, thickness and coating (up to 1mm thick) and is effective for both artificial and in service corrosion style defects, in terms of their detection and axial sizing and approximate circumferential positioning of a defect. Simulated data has been shown to match the experimental measurements and the model can be used to investigate further the effects of changing defect depths, geometry and generation and detection points without the need to generate new samples of which the exact defect geometry is known.

However, the inspections presented here are limited by the requirements placed on the inspection equipment. Due to the scans being carried out in situ, the pulser electronics have to be portable and battery powered and the probes must have a limited footprint and size. This limits both the number of cycles in a tone burst available for inspections and the wavelength bandwidth of the transducers. The combination of these restrictions makes it difficult for a single mode to be selected and individually excited. As a consequence of this at least two different modes are excited each time, which complicates the signals due to the similarity in speeds of the different modes and their proximity in the resulting time records.

Modelling of defects in pipes has also shown that the slope of the defect edges and the depth of the defect dictates how the signals propagate into and away from the defect. A defect that has an abrupt start for example but a remaining depth that doesn’t go below the

SH1 cut off thickness could still redistribute much of the energy in the SH1 mode in reflections from the defect edge.

It is apparent that consideration of the encoded image scans that the system automatically generates is not sufficient to fully characterise a defect. Qualitative analysis of the data is necessary in order to accurately axially size the defect area and confirm what is happening to the redistributed signal in the sample.

This technique has been shown to be effective for rapid screening of pipe samples and is capable of finding small defects by comparison with clear areas of the sample. The general complexity of in service defects in terms of the overall shape of the defect, the depth profile throughout a wall thinning defect and the nature of the defect edge sharpness, all contribute to the varying degrees of reflection and mode conversion of the incident modes. Accurate reconstruction of the defect profiles is not always possible.

It is intended that the experimental work here and the generation of a feasible model of the same could be used to compare to further data from known defects and blind trials to give a catalogue of defects and how they affect signals in order to aid defect identification in the future.

8. Acknowledgments

This work is funded by the Engineering and Physical Sciences Research Council (EPSRC) through an EngD studentship from the Research Centre for Non Destructive Evaluation, Grant EP/F017332/1 and supported by Sonomatic Ltd.

References

[1] McCafferty E. Introduction to Corrosion Science. New York, NY: Springer New York; 2010.

[2] Cosham A, Hopkins P, Macdonald K A. Best practice for the assessment of defects in pipelines – Corrosion. Eng Fail Anal 2007;14:1245–65.

[3] Alleyne DN, Cawley P. The interaction of Lamb waves with defects. IEEE Trans Ultrason Ferroelectr Freq Control 1992;39:381–97.

[4] GE pipe integrity services: crack detection. (GE Oil and Gas) [Online] Available https://www.geoilandgas.com/pipeline-storage/pipeline-integrity-services/crack-management. [Accessed 24 Aug 2015] 2014

[5] Evaluation of the effectiveness of non-destructive testing screening methods for in-service Inspection. (HSE Res Report) [Online] Available http//www.hse.gov.uk/research/rrpdf/rr659.pdf [Accessed 24-Aug-2015] 2009.

[6] Løvstad A, Cawley P. The reflection of the fundamental torsional guided wave from multiple circular holes in pipes. NDT E Int 2011;44:553–62.

[7] Zhao X, Varma VK, Mei G, Ayhan B, Kwan C. In-Line Nondestructive Inspection of Mechanical Dents on Pipelines With Guided Shear Horizontal Wave Electromagnetic Acoustic Transducers. J Press Vessel Technol 2005;127:304.

[8] Hirao M, Ogi H. An SH-wave EMAT technique for gas pipeline inspection. NDT E Int 1999;32:127–32.

[9] Ribichini R, Nagy PB, Ogi H. The impact of magnetostriction on the transduction of normal bias field EMATs. NDT E Int 2012;51:8–15.

[10] Ribichini R, Cegla F, Nagy P, Cawley P. Study and comparison of different EMAT configurations for SH wave inspection. IEEE Trans Ultrason Ferroelectr Freq Control 2011;58:2571–81.

[11] Dixon S, Petcher P a, Fan Y, Maisey D, Nickolds P. Ultrasonic metal sheet thickness measurement without prior wave speed calibration. J Phys D Appl Phys 2013;46:445502.

[12] Velsor J Van. Circumferential guided waves in elastic and viscoelastic multilayered annuli. Penn State University PhD thesis, 2011.

[13] Zhao X, Rose JL. Guided circumferential shear horizontal waves in an isotropic

hollow cylinder. J Acoust Soc Am 2004;115:1912.

[14] Liu G, Qu J. Guided Circumferential Waves in a Circular Annulus. J Appl Mech 1998;65:424. doi:10.1115/1.2789071.

[15] Nakamura N, Ogi H, Hirao M, Nakahata K. Mode conversion behavior of SH guided wave in a tapered plate. NDT E Int 2012;45:156–61.

[16] Nurmalia N, Nakamura N, Ogi H, Hirao M. Detection of Shear Horizontal Guided Waves Propagating in Aluminum Plate with Thinning Region. Jpn J Appl Phys 2011;50:07HC17.

[17] Uribe S. A, Nakamura N, Ogi H, Hirao M, Thompson DO, Chimenti DE. Mode Conversion of SH Guided Waves At Defects for Pipeline Inspection. AIP Conf Proc 2009;1550:1550–7.

[18] IEEE Instrumentation and Measurement (I&M) Society, IEEE Standard on Transitions, Pulses, and Related Waveforms. IEEE Std 181-2003;2003.